Received: 12 June 2022 | Revised: 11 September 2022 | Accepted: 13 September 2022

DOI: 10.1002/est2.412

RESEARCH ARTICLE

ENERGY STORAGE WILEY

Charging characterization of a high-capacity lithium-sulfur pouch cell for state estimation: An experimental approach

Neda Shateri | **Daniel J. Auger** | **Abbas Fotouhi** | **James Brighton**

Advanced Vehicle Engineering Centre, Cranfield University, Bedfordshire, UK

Correspondence
Neda Shateri, Advanced Vehicle Engineering Centre, Cranfield University, Bedfordshire, MK43 0AL, UK.
Email: neda.shateri@cranfield.ac.uk

Funding information
Innovate UK; European Commission

Abstract

Lithium—Sulfur (Li—S) battery is a next-generation technology, which is promising for applications that require higher energy density in comparison to the available lithium-ion batteries. Along with the ongoing research on Li—S cell material development and manufacturing to improve this technology, engineers are also working on Li—S battery management systems (BMS). The existing BMS algorithms, which are developed for lithium-ion batteries, are not useable for the Li—S mainly due to its constant voltage plateau during the discharge phase. As a result, the Li—S system has poor observability during discharge, which limits the BMS functionality that can be implemented from discharge information alone, and it is worth considering if information from charging is useful. In this study, the charging behavior of a high-capacity pouch cell is investigated and characterized for the purpose of state estimation in a BMS. Several tests are conducted on prototype Li—S cells at different temperatures and age levels. An online feature extraction method is then used in combination with a classification technique to estimate the cell's states during charging. The proposed charging estimators can provide accurate initialization for state estimation accuracy during discharge by providing good estimates of the post-charging state of charge (ie, around 3%) and capacity after fading (ie, around 2%).

KEYWORDS

characterization, charging, feature extraction, lithium-sulfur battery, state estimation

1 | INTRODUCTION

Weight is an important feature of a battery system, which means the need for high gravimetric energy densities. One of the promising technologies to achieve that goal is the lithium—sulfur (Li—S) battery.[1,2] In comparison to the extant lithium-ion battery technologies in the market, Li—S offers some superiorities such as higher energy density (theoretically up to 2600 Wh/kg),[3] enhanced safety, and less cost because of the wide availability of sulfur in nature. However, there are still a few impediments to the full commercial development of this technology such as less power capability, higher self-discharge, and shorter cycle life.[4] It should be also mentioned that there have been lots of achievements in further development of Li—S cells in recent years.[5-7] An example of such achievements is presented in Reference [8], where a Li—S cell with more than 1000 cycles is mentioned. Alongside the

ongoing research on the cell material and manufacturing, engineers are also trying to develop battery management system (BMS) for Li—S batteries.[9]

According to the control theory and based on what is presented in Reference [10], the Li—S cell's model is not observable as we expect for other battery types. That outcome means it is more difficult to control the Li—S battery in comparison to the other battery types via a BMS board.[11,12] For example, Figure 1 demonstrates a comparison between the charge/discharge voltage curves of a Li—S cell and a lithium nickel cobalt aluminum oxide (NCA) cell. As shown in figure, the voltage gradient, which is clearly observed in an NCA cell, does not exist in some regions of the Li—S cell voltage curve (ie, around 30%-70% charge). Although having a flat voltage curve might be an advantage in some aspects, it makes the system more complicated in terms of observability and controllability.

The engineering efforts to develop a suitable BMS for Li—S battery, have been addressed in a few previous studies mainly focusing on state-of-charge (SoC) and state-of-health (SoH) estimation algorithms. However, more research is required in that field. Looking at Li—S battery literature, there are few studies in which SoC estimation techniques are developed for Li—S battery and that research area is still open. In References 13,14, Kalman filter-based SoC estimators are modified to be applicable for Li—S cells. In another study, an adaptive neuro-fuzzy inference system (ANFIS) is used for SoC estimation of a Li—S cell.[9] In a similar approach, ANFIS was replaced by a support vector machine (SVM) in Reference [15] to perform the same using an electrical circuit model and system identification. In some other recent studies presented in References [16,17], the possibility of using a reduced order electrochemical Li—S cell model for the estimation of SoC is investigated as well. In none of the above-mentioned studies, the charging process of Li—S battery is considered, which distinguishes this study from the literature.

Despite the remarkable studies on the reasons behind the Li—S cell degradation mechanisms, there are not enough studies on SoH estimation for BMS application. In References [18,19], an experimental approach is used to analyze the Li—S cell's aging to be used in BMS. In another study,[20] capacity fade and internal resistance of a 3.5 Ah Li—S cell is investigated using test data. A more comprehensive study on the performance degradation of the Li—S cell is presented in Reference [21] where a high-capacity Li—S cell is subjected to degradation tests, and all parameters of an electrical circuit model are investigated during the discharge phase, subject to aging.

As mentioned above, in none of those studies, the charging process of Li—S battery is regarded to be used in BMS. The battery state estimators, which are developed to work during charging, could be investigated as complementary algorithms in a BMS. Since battery discharge patterns might change significantly from an application to another, the state estimators' performance is affected by the varying discharge profile. However, in this study, the battery charging profile is considered instead to achieve a more robust state estimation result. Particularly for Li—S battery, it makes even more sense to do the estimations during charging because of the more complex behavior of Li—S battery during the discharge process.

This study investigates the charging behavior of a high-capacity Li—S pouch cell and its characterization for state estimation in BMS. A data-driven approach, based on charging feature extraction, is used which is new for Li—S battery. In Reference [22], a good comparison between different data-driven battery state estimation

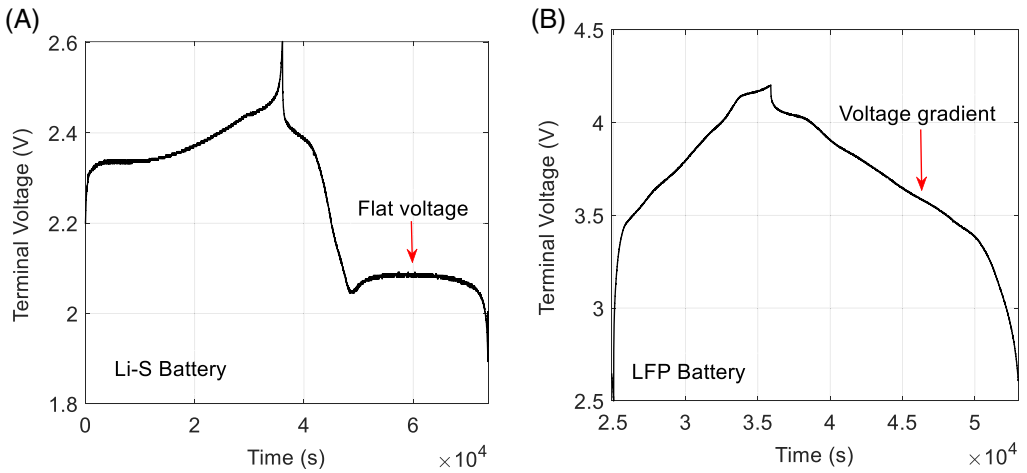

FIGURE 1 Comparison between charge/discharge voltage curves of Li—S and nickel cobalt aluminum oxide (NCA) cells: the voltage gradient, which is observed in Li-ion cells, does not exist in some regions of Li—S state-of-charge (SoC) (30%-70%)

algorithms is discussed. Among them, the SVM method is found as an effective method in the literature[23-26] because of its speed as well as accuracy. Therefore, the SVM method is selected and used in this study in combination with the charging feature extraction technique.[27,28]

The novelties of this work can be listed as follows:

- For the first time, the charging behavior of the Li—S cell is investigated and characterized for state estimation.
- A state-of-the-art Li—S cell is tested by running a comprehensive set of experiments at different temperature and age levels.
- A state observability analysis is performed for the Li—S cell to mathematically demonstrate its difference from the other types of battery.
- New state estimators are designed and validated to be used during Li—S cell charging, as a complementary algorithm in BMS.
- Capacity fade and charging efficiency of the prototype cells are analyzed based on experimental data.

The objectives of the present work are:

1- To investigate and analyze the Li—S cell charging behavior using an experimental approach.
2- To perform an observability analysis on Li—S state of charge estimation.
3- To design and validate new state estimation techniques to be used for Li—S cell during charging.

2 | LI—S CELL MODELING AND OBSERVABILITY ANALYSIS

2.1 | Li—S cell modeling

The prototype Li—S pouch cell that is investigated in the present work, is provided by OXIS Energy Ltd.[29] The cell's features are presented in Table 1. The cell has a very low internal resistance, which makes it different from others in the literature. The previous Li—S pouch cells, which have been investigated in References [12-14] had a nominal capacity of 3.4 Ah whereas the present one has a nominal capacity of 19 Ah. Here, the parameters of an electrical circuit model, called the Thevenin model,[30] are obtained using the charge/discharge data of the cell. As shown in Figure 2A, the Thevenin model has four parameters, which include the cell's open-circuit voltage (V_{OC}), ohmic resistance (R_O), polarization resistance (R_P), and polarization capacitance (C_P). The other variables shown in the figure are the load current (i_L) and terminal voltage (V_t), which are measured as the model's input and output, respectively. The mathematical equations of the Li—S cell model are:

TABLE 1 Li—S cell features

Parameter	Value
Cell capacity	19 (Ah)
Cell mass	141 (g)
Maximum voltage	2.6 (V)
Nominal voltage	2.15 (V)
Minimum voltage	1.9 (V)
Maximum discharge rate	3°C–57(A)
Maximum charge rate	0.25°C–4.75 (A)

$$\begin{cases} V_t = V_{OC} - R_O I_L - V_p \\ \dfrac{dV_p}{dt} = -\dfrac{1}{R_p C_p} V_p + \dfrac{1}{C_p} I_L \end{cases} \quad (1)$$

A system identification method, called forgetting factor recursive least-squares (FFRLS),[31] is used to parameterize the Thevenin model according to the test data. As a result, the model's parameters (included in vector $\boldsymbol{\theta}$) is found so that the following error function (ε) is minimized.

$$\varepsilon(t_k, \boldsymbol{\theta}) = V_t(t_k) - \hat{V}_t(t_k | t_{k-1}; \boldsymbol{\theta}) \quad (2)$$

$$\boldsymbol{\theta} = [V_{OC}, R_O, R_P, C_P] \quad (3)$$

where $V_t(t_k)$ is the measured terminal voltage in step k and $\hat{V}_t(t_k|t_{k-1};\boldsymbol{\theta})$ is the estimated voltage in step k using $\boldsymbol{\theta}$. Since the estimation error is a function of $\boldsymbol{\theta}$, an iterative optimization procedure is necessary. Because the cell model parameters depend on SoC as well, the whole identification process should be repeated at different charge levels. Figure 2B depicts an example identification result during a discharge test, starting from fully charged state (100% SoC) until a complete charge depletion (0% SoC). On the other hand, Figure 2C illustrates another example starting from 60% SoC. According to the results, the system identification algorithm is able to identify the model's parameters, however, the state of the system is unknown. Assume a case in which the initial SoC is unknown; then how can we estimate the system's state just at the beginning? That is especially important when the initial SoC is somewhere in the middle (around 30%-50%) because the voltage curve is totally flat in that region. In real life, there are several situations in which

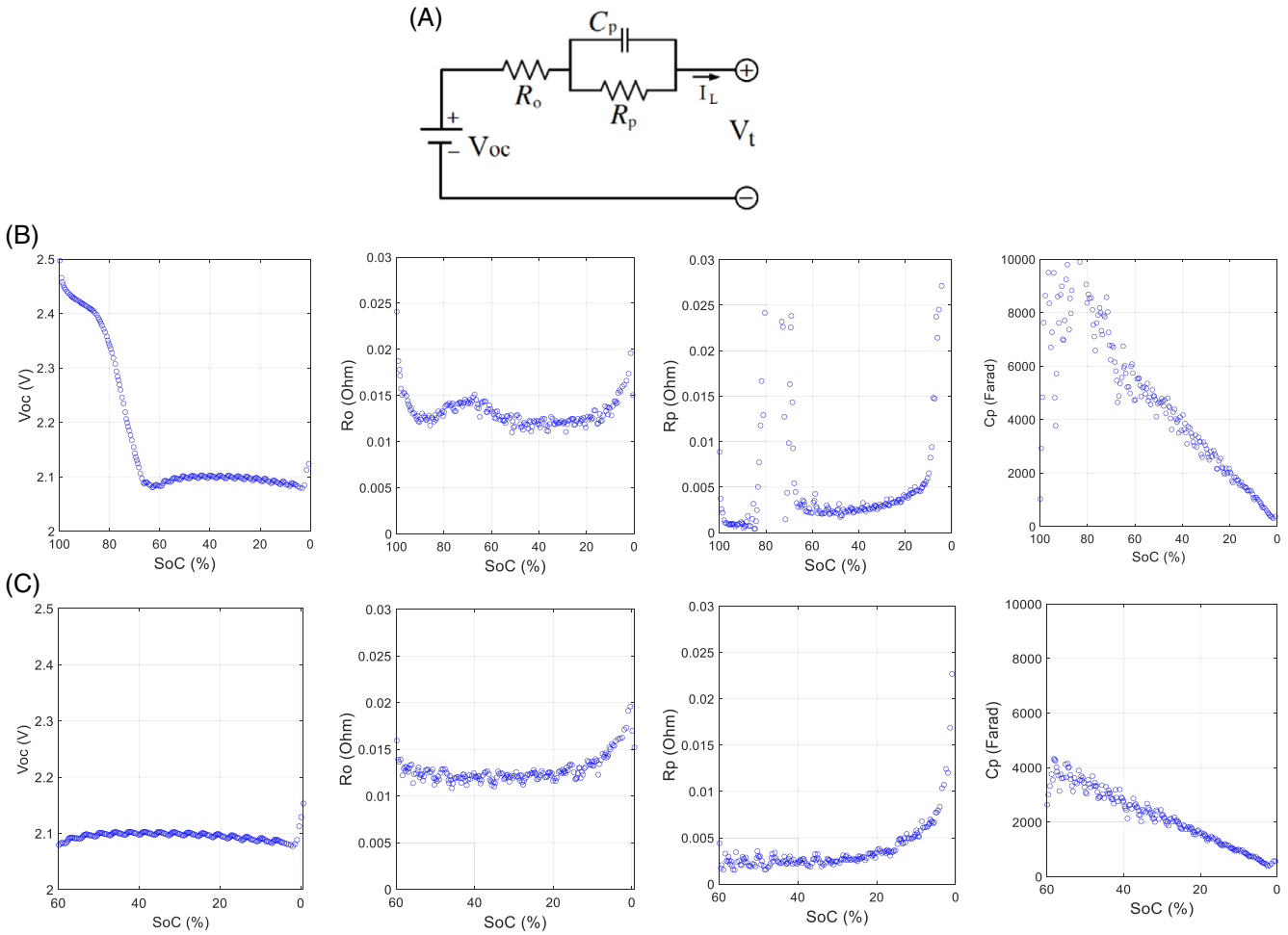

FIGURE 2 Thevenin battery model and its parameters (V_{OC}, R_O, R_P, and C_P) identified for a Li—S cell at different state-of-charge (SoCs): (A) model structure, (B) initial SoC = 100%, (C) initial SoC = 60%

an EV or a cell phone is not fully charged by the user, and the question is: can we have an accurate state estimator during the charging phase? That is critically important for Li—S battery because all the existing state estimators of Li—S [13-15] are focused on the discharge phase only. In the following section, an analytical formulation is presented to mathematically show that the Li—S Thevenin model is not observable based on the control theory. That fact motivated the authors to develop state estimators which are specifically useful during the charging phase of Li—S battery. Such algorithms can be used as a complementary part beside the existing discharge state estimators in a Li—S BMS.

2.2 | Observability analysis

To mathematically investigate the impact of Li—S cell's flat voltage curve on its state observability, a more general formulation of the Thevenin model can be represented in the state-space form as follows.

$$\begin{aligned} \boldsymbol{y}(t) &= \boldsymbol{C}\boldsymbol{x}(t) + \boldsymbol{D}\boldsymbol{u}(t) \\ \dot{\mathbf{x}}(t) &= \mathbf{A}\mathbf{x}(t) + \mathbf{B}\mathbf{u}(t) \end{aligned} \tag{4}$$

where $\mathbf{y}(t) \in R^N$ and $\mathbf{u}(t) \in R^M$ are the vectors of outputs and inputs, respectively, $\mathbf{x}(t) \in R^K$ is a time-dependent state vector, and the matrices $\mathbf{A} \in R^{K\times K}$, $\mathbf{B} \in R^{K\times M}$, $\mathbf{C} \in R^{N\times K}$, and $\mathbf{D} \in R^{N\times M}$ define the system's behavior.

Assume a variable X to denote the battery SoC. Based on the Thevenin model's equations in (1), V_P and X can be considered as the model's states whereas the load current and the battery terminal voltage are the input and output, respectively. Now the model's equations should be rewritten in the standard state-space format. According to the concept of coulomb-counting, the first state variable (ie, SoC) is formulated as integration of the load current over time. For the second state variable, V_P, the second part of Equation (1) can be used without any change. In the first part of Equation (1) however, the open-circuit voltage (V_{OC}) must be presented as a function of SoC. According to Figure 2, V_{OC} has a nonlinear

function vs SoC. Such a nonlinear function can be linearized locally within a limited range of SoC. Assuming small SoC intervals, Δ_{SoC}, V_{OC} can be presented as follows in the ith SoC interval.

$$V_{oc} = a_i.X_i + b_i, \quad (i-1).\Delta_{SoC} \le X_i \le i.\Delta_{SoC} \tag{5}$$

The coefficients a_i and b_i need to be calculated for each range of SoC separately. Figure 3 shows a schematic of the piecewise linearization procedure of Li—S cell's charge/discharge voltage curves. Although the plot is showing the terminal voltage, the shape of V_{OC} curve is very similar because the load current is low (refer to Figure 2). The resolution might be higher or lower by changing the size of SoC intervals. Indeed, here the goal is not to calculate such piecewise linear functions, but this study aims at showing something else as discussed below.

When we replace V_{OC} by its linearized approximation, in Equation (1), we have:

$$V_t = a_i.X + b_i - R_o I_L - V_p \tag{6}$$

And a state-space representation of the cell model is achieved.

$$\begin{cases} \begin{bmatrix} \frac{dV_p}{dt} \\ \frac{dX}{dt} \end{bmatrix} = \begin{bmatrix} -\frac{1}{R_p C_p} & 0 \\ 0 & 0 \end{bmatrix} \begin{bmatrix} V_p \\ X \end{bmatrix} + \begin{bmatrix} \frac{1}{C_p} \\ \frac{\eta}{C_t} \end{bmatrix} I_L \\ V_t - b_i = [-1 \ a_i] \begin{bmatrix} V_p \\ X \end{bmatrix} - R_o I_L \end{cases} \tag{7}$$

In control theory, such a state-space system is called "observable" if the observability matrix, $\mathbf{W}_o$, has full column rank,[32] where K is the state vector's dimension.

$$\mathbf{W}_o := \begin{bmatrix} \mathbf{C} \\ \mathbf{CA} \\ \mathbf{CA}^2 \\ \vdots \\ \mathbf{CA}^{K-1} \end{bmatrix} \tag{8}$$

In our case, the Li—S cell model's observability matrix is:

$$\mathbf{W}_o := \begin{bmatrix} C \\ CA \end{bmatrix} = \begin{bmatrix} -1 & a_i \\ \frac{1}{R_P C_P} & 0 \end{bmatrix} \tag{9}$$

Because parameters R_P and C_P have positive non-zero values, $\mathbf{W}_o$, is always full rank except when a_i becomes zero. According to Figure 1, that condition never happens for an NCA cell model because of its voltage curve, which has a gradient all the time. However, looking at Figure 3, the state observability of the Li—S cell model is not provided because the parameter a_i becomes zero at some points on the voltage curve. That is an important characteristic of Li—S cell, which makes it different from other battery types not only with respect to its electrochemical reactions but also in terms of its observability in the control theory.

3 | LI—S CELL CHARGING VOLTAGE CURVE ANALYSIS

3.1 | Li—S cell testing and charging feature extraction

In this section, the charging voltage curve of the cell is investigated based on the experimental data. The test equipment, which is used in this study, is shown in Figure 4A. The test rig includes a PC to design the battery

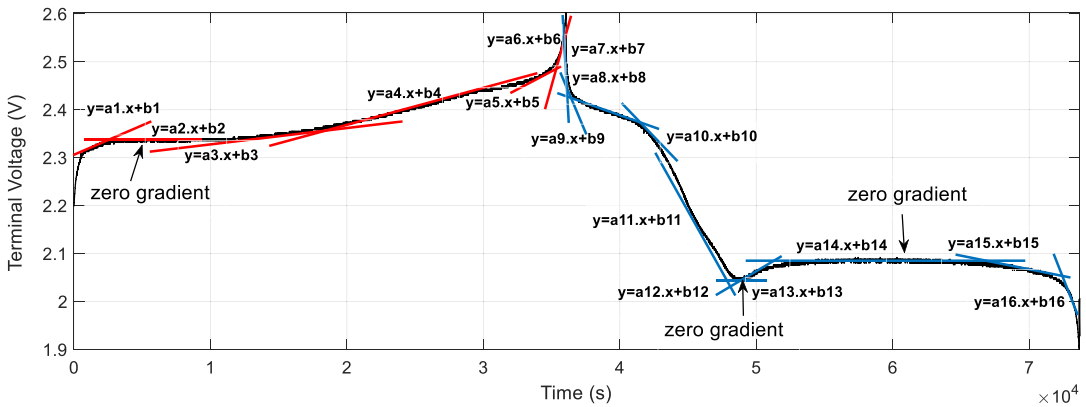

FIGURE 3 Li—S cell charge/discharge voltage curve piecewise linearization

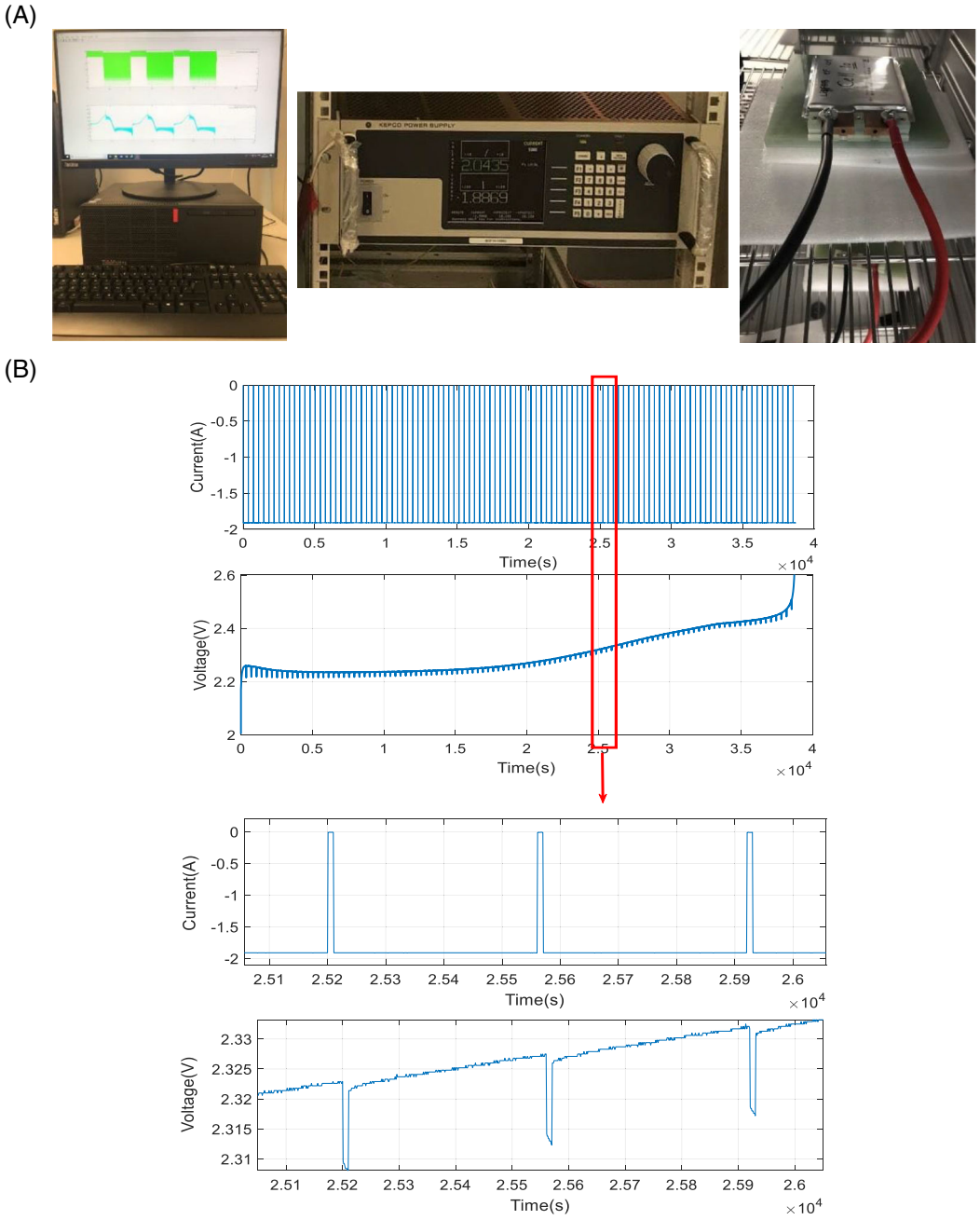

FIGURE 4 Li—S cell charge test: (A) equipment and (B) measurement

test procedure as well as the data storage, a power source that applies the charging current, and an environmental chamber to control the temperature during the tests. As depicted in Figure 4B, the cell is subjected to a full charge cycle from 0% to 100% SoC based on the minimum and maximum voltage limits. Accordingly, cell charging curve analysis would be possible at different SoC levels. After each charge cycle, the Li—S cell is discharged again making it ready for the next cycle. At each charge cycle, a constant current of 1.9 A (ie, 0.1C for a single cell - this is expected to be scaled up for a battery pack) is applied to the cell based on a recommendation by the cell's manufacturer. Moreover, to extract additional data from the charging profile, short relaxations (around 10 s) are considered at regular time intervals, illustrated in Figure 4(B). Applying that technique in a real application does not need to be repeated many times as we did in the laboratory environment. In fact, after identifying particular SoC target points, the relaxation pulses can be applied only a few times when needed (ie, a design parameter in the BMS).

Two groups of features are extracted from the Li—S cell charging voltage profile: (a) instantaneous voltage features (IVFs) and (b) time-voltage features (TVFs). In

the first group, the features are defined based on battery voltage response to the short current relaxation pulse. The reason for choosing a short time interval (ie, 10 seconds), is to be able to implement the estimators in real-time without causing any delay in the charging process. As shown in Figure 5, the first feature, F1, represents the battery terminal voltage before releasing the charging current. Feature F2 is the battery voltage at the end of each 10-second relaxation period. Features F3 and F4 are instantaneous voltage drop and jump after release and reapply of the charging current respectively. Furthermore, feature F5 is the slow drop of voltage over 10 seconds during the relaxation period, and feature F6 is the slow rise of voltage after 10 seconds of reapplying the charging current as shown in Figure 5.

Figure 6 shows the second group of features, which are called TVFs. The TVFs are proposed based on the time duration of different intervals of voltage when the Li—S battery is subjected to charging as shown in Figure 6. It should be noted that constant-current charging is the recommended way of charging Li—S prototype cells by the manufacturer. According to Figure 6, the Li—S cell's terminal voltage changes between 2.2 and 2.6 V while getting charged. According to the test results, the gradient of the voltage-time curve is not constant. Six features are defined (ie, $F_7 - F_{12}$) based on equal voltage intervals from 2.25 to 2.55 V, which are the time duration of voltage change at each interval. The whole charging process takes around 10 hours in total, and the time axis is presented in minutes in Figure 6 to better see the duration of each interval. Numerical values of all the IVFs and TVFs are analyzed in the following sections for state estimation during charging.

3.2 | The effect of temperature on Li—S cell charging features

The influence of the temperature on cell's charging features is investigated here by repeating the above-mentioned feature extraction technique at 10°C, 20°C, and 30°C. An environmental chamber is used to keep the temperature constant during the tests. Figure 7 shows Li—S cell IVFs, which are recorded at different levels of SoC and temperature. According to the results, the temperature has a different impact on each feature and its impact depends on SoC as well. According to Figure 7, the highest gradient vs SoC is observed for features F1 and F2, which means they are more sensitive to SoC variation. On the other hand, F3 and F4 are the least sensitive features with respect to SoC. In terms of the temperature effect, F1 and F2 are more affected in the higher SoC range whereas no clear impact is observed in F3 and F4 when the temperature changes. For features F5 and F6, the temperature has a clearer impact on them where the highest feature values are obtained at the lowest temperature (ie, 10°C).

Figure 8 shows the effect of temperature on the Li—S cell TVF charging features. Three charging voltage curves are illustrated in Figure 8A at 10°C, 20°C, and 30°C. The

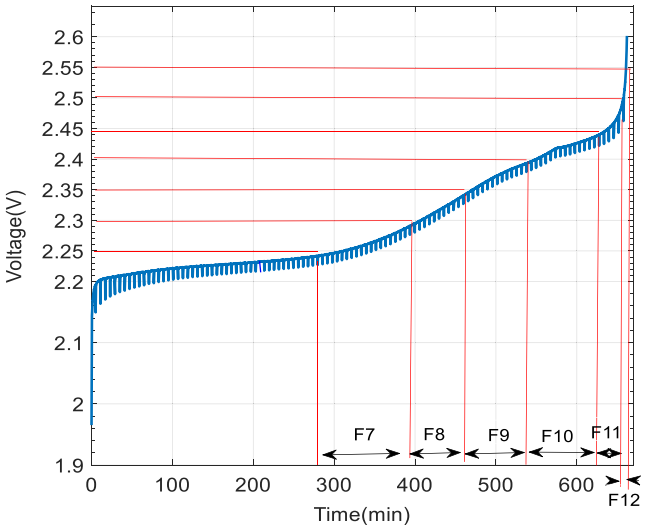

FIGURE 6 Li—S cell charging voltage profile and definition of time-voltage features (TVFs)

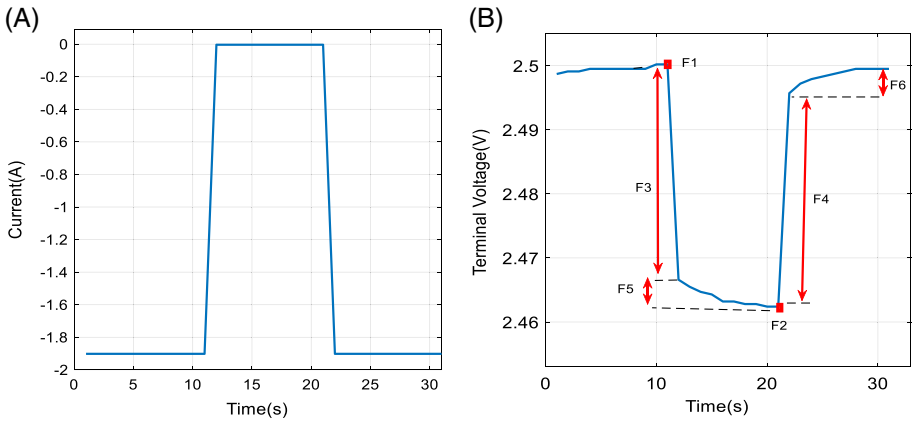

FIGURE 5 (A) A 10-second relaxation pulse between constant charging, (B) Li—S cell's voltage response to a single relaxation pulse and definition of instantaneous voltage features (IVFs)

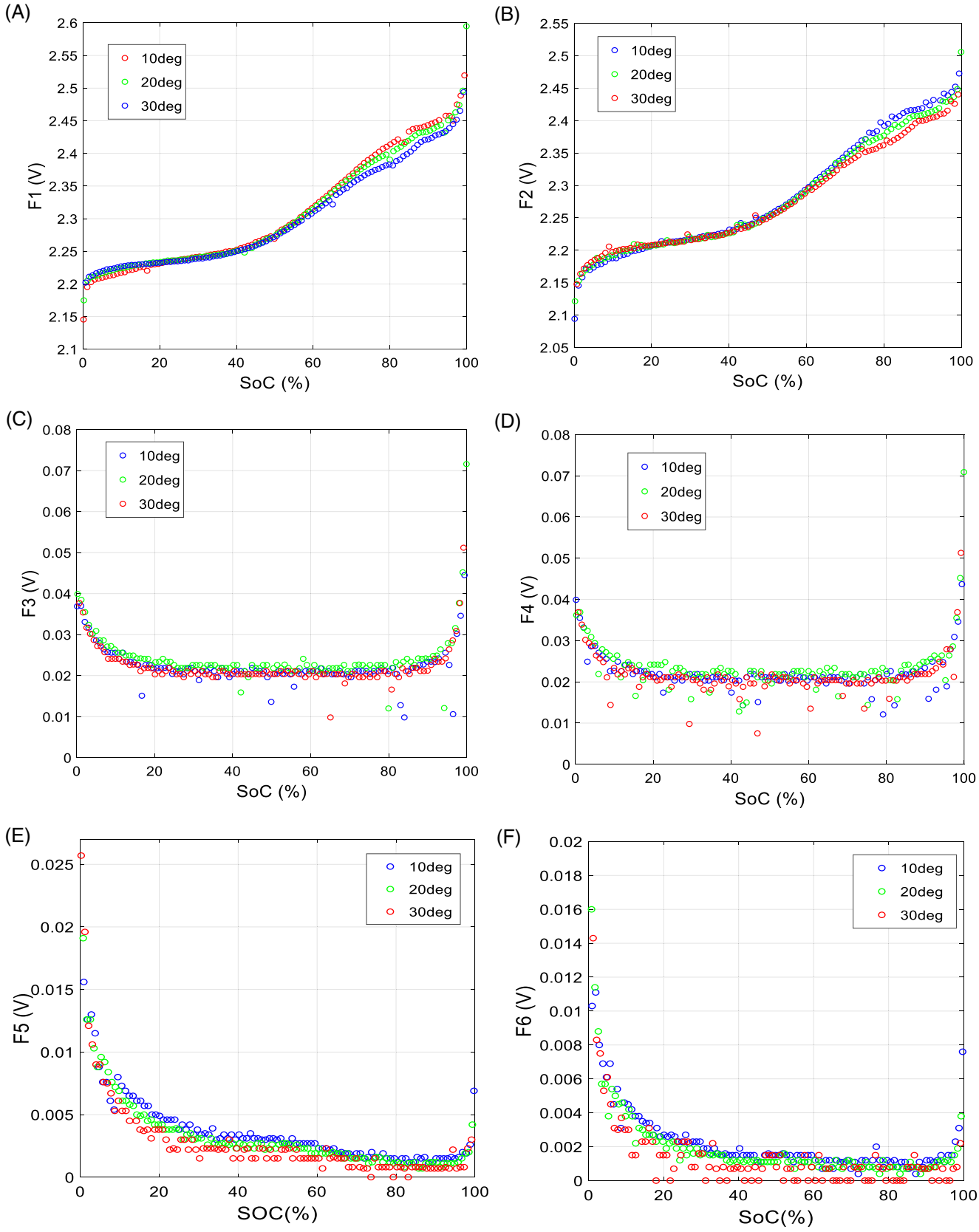

FIGURE 7 Li—S cell instantaneous voltage features (IVF) charging features recorded at different levels of state-of-charge (SoC) and temperature

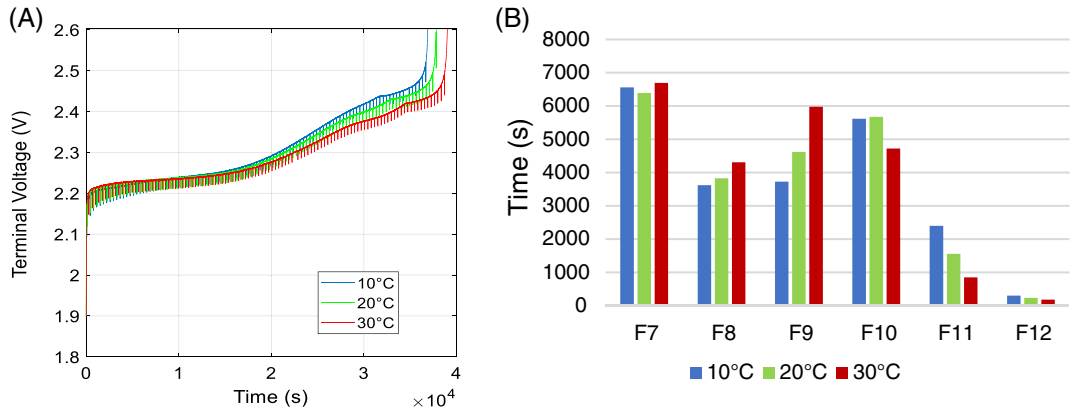

FIGURE 8 The influence of temperature on Li—S cell time-voltage features (TVF) charging features: (A) charging voltage curves, (B) TVF values

first outcome is that a higher temperature is led to higher charging capacity and consequently longer charging time. Because TVFs are strongly correlated with the charging time as well as the voltage change, it is expected to observe an impact on them as well. Figure 8(B) summarizes the effects of temperature on the TVFs. According to the results, various features are affected in different ways. For example, F7 does not show any influence by the temperature change. Looking at the charging curves in Figure 8A, an interesting outcome is that the first half of the Li—S cell's charging curve (ie, 0-50% SoC approximately) is not affected by the temperature change that much, whereas more change is observed in the second half. That is why we do not see any temperature sensitivity in F7. For F8 and F9, a temperature rise increases their values mainly because of the longer charging time. However, that trend changes for F10, F11, and F12 where they decrease in response to temperature rise. That is because the voltage shifts up and down at high SoCs when the temperature decreases or increases, respectively.

3.3 | The effect of degradation on Li—S cell charging features

In this section, the influence of cell degradation on its charging features is investigated. Two age levels are considered and compared: (a) a fresh cell, and (b) an aged cell. Figure 9 shows Li—S cell IVFs, which are recorded at different levels of SoC and age. The results demonstrate that the aging process has different impacts on various features. For example, for features F3 and F4, although the gradient vs SoC is unchanged, the whole curve is shifted up due to cell aging. That is not helpful for SoC estimation, however, we will discuss it in Section 5 where the cell's SoH estimation becomes our goal. For features F5 and F6, an increase is observed due to aging, however, it is not as much as those of F3 and F4. On the other hand, F1 and F2 are not showing a clear trend of change in response to cell cycling. That means F1 and F2 are not suitable features for cell SoH estimation, however, that makes them perfect for SoC estimation as discussed in Section 4.

Figure 10 shows the influence of aging on the TVF charging features. Figure 10A compares two charging curves of a fresh and an aged cell. The first outcome is that the aging process has reduced the charging time, which is explained by the capacity fade due to cycling. The second outcome is related to voltage increase due to aging, which can be explained by the increase in the cell's internal resistance due to cycling. As a result, for most of the features (ie, F7-F10), TVFs reduce by aging because of the shorter charging time. However, F11 and F12 are showing a slight increase due to the voltage shift at high SoCs (similar to what was observed for the temperature effect in Figure 8).

4 | LI-S CELL SOC ESTIMATION DURING CHARGING

As discussed earlier, the Li—S battery SoC estimation problem is a demanding task and therefore, the current battery estimation techniques are not necessarily useable for it.[9,12] To solve that problem, the present study was aimed at investigating Li—S cell charging behavior to support state estimation in BMS. After defining and analysis of the Li-S cell charging features, in this section, the possibility of their use in cell SoC estimation is investigated. For that purpose, the SVM technique[33,34] is used to receive the charging features as inputs and to return the Li—S cell SoC as its output.

Various combinations of the input features are considered to train the SVM model. It should be mentioned that separate sets of data are used for training and

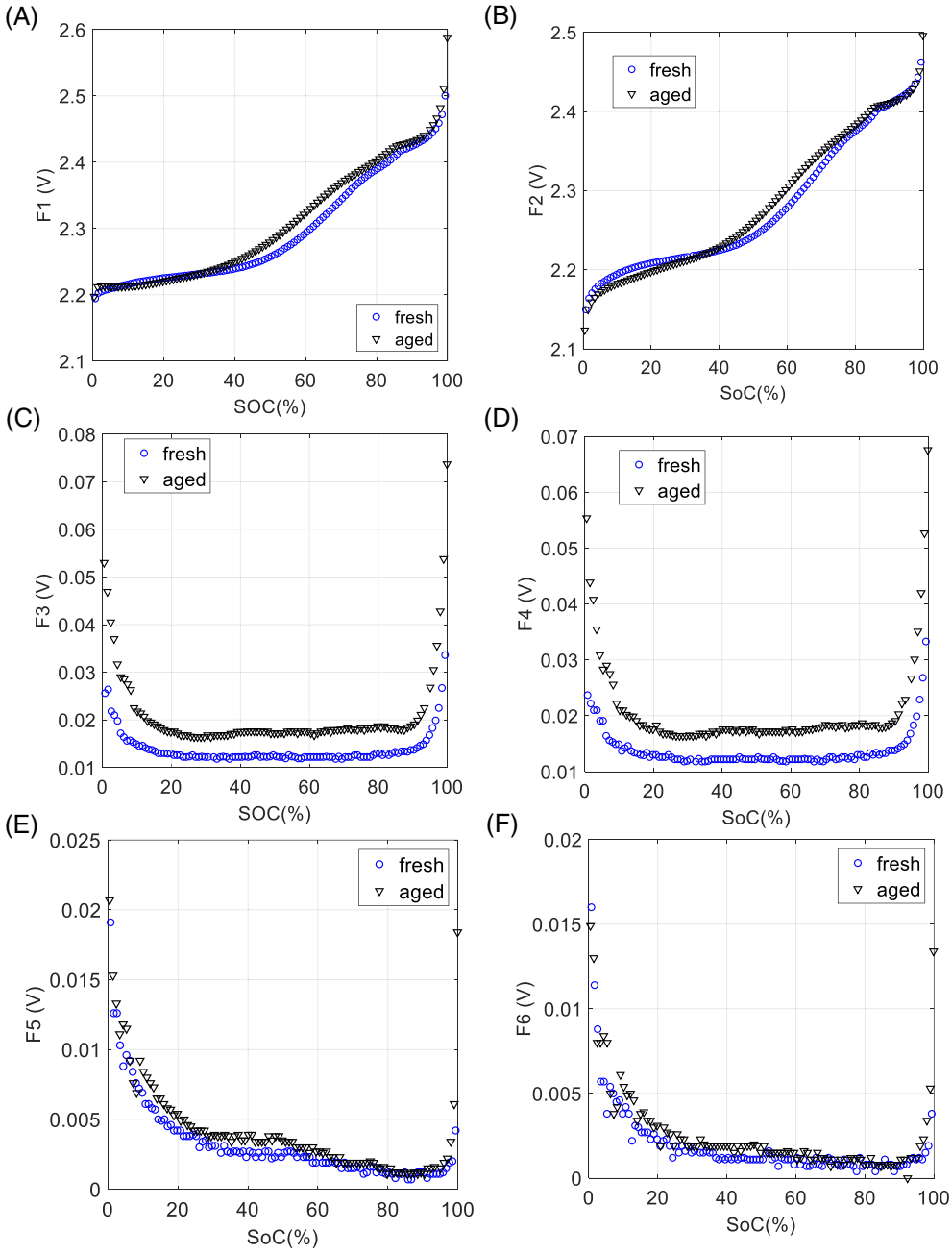

FIGURE 9 Li—S cell charging features recorded at different age levels

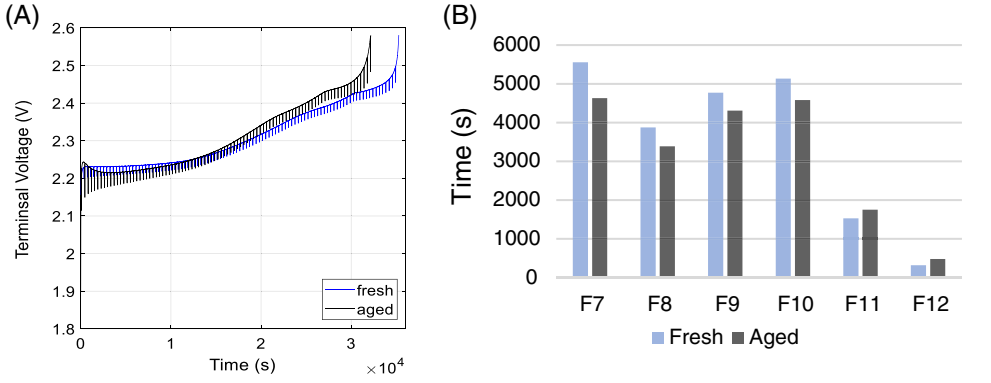

FIGURE 10 The effect of aging on the time-voltage features (TVF) charging features: (A) charging voltage curves, (B) TVF values

validation. To calculate the "true SoC," the coulomb-counting formulation is used for offline training of the SVM model. The coulomb-counting technique suffers from limitations like accumulated noise error.[35,36] In addition, the coulomb-counting method needs to know the initial SoC as well as the battery capacity (which changes under different conditions). Consequently, while we are aware of the practical limitations of having access to the true SoC labels in real applications, in this study, it is only used as a benchmark for validation purposes in a laboratory environment.

All charging features are investigated one by one to identify the inputs that give the highest SoC estimation accuracy. According to the results, some features like F1 and F2 contribute more to the SoC estimation accuracy. That outcome can be easily explained when looking at Figure 7 or Figure 9 where the gradients of F1 and F2 vs SoC are quite strong. The opposite outcome is obtained for features F3 and F4, which have the least gradient vs SoC (again based on Figure 7 or Figure 9), showing that those two features are not sensitive to SoC change. On the other hand, the TVFs (ie, F7-F12) are not practical for SoC estimation because of the time which is required for their calculation. In fact, those features were defined to be used mainly for SoH estimation rather than SoC estimation. This topic is discussed further in Section 5.

Figure 11 illustrates an example of Li—S cell SoC estimation result using SVM during charging at 20°C. An average error of 2.71% is achieved in that case. The proposed SoC estimator is designed to start from an initial value of 50% SoC when no history is available (ie, only for the first iteration). For performance evaluation of the proposed estimator, the "theoretical" coulomb-counting method is used as a benchmark, which is called the "true SoC" or the "reference SoC."

In order to consider the effect of temperature, a separate estimator can be trained using the data collected at that specific temperature. In real-time applications, switching between those estimators is possible based on temperature sensor data. In that technique, the operational temperature range is designed first (eg, between 10°C and 30°C) and then, it is discretized into smaller regions (let say 10°C intervals). After that, separate estimators are tunned suitable for different temperature regions.

5 | LI—S CELL STATE-OF-HEALTH ESTIMATION DURING CHARGING

In this section, Li—S cell's state-of-health (SoH) is studied, and a method is proposed for online SoH estimation of Li—S cells during charging. For that purpose, charge/discharge tests are repeated until the cells are degraded based on their capacity fade. To analyze the degradation process, firstly the IVFs and TVFs are obtained at different cycles (ie, age levels). Then an SVM model is trained using Li—S cell test data, to act as a SoH estimator. There are several other battery SoH estimation techniques in the literature, which could be potentially used here as well. However, applying all the available techniques is not possible here, and the goal of this study is not to review and compare different methodologies. So, potential further improvement of the results by applying other techniques is left for future work.

The SoH is defined as a number between zero and one, where SoH = 0 means the battery's end-of-life (EoL), and SoH = 1 corresponds to a fresh battery. To be able to measure the reference value of SoH, first, the battery EoL should be defined. In many applications, the battery health is evaluated based on its capacity (Q_{batt}) against the initial capacity (Q_{init}). In that definition, the EoL happens when the capacity reaches to 80% of the initial capacity as presented below.

$$\mathrm{SoH} = 1 - (Q_{init} - Q_{batt})/0.2^{*}Q_{init}, \quad 0.8\,Q_{init} \le Q_{batt} \le Q_{init} \tag{10}$$

The SoH value which is obtained by Equation (10), is called "reference SoH" or "true SoH." The reference SoH value is obtained according to the experimental test data. In fact, the reference SoH is obtained after completing all the experiments and analysis of them. We know that such data is not available in a real application however, we can use it as a benchmark in a laboratory environment just for validation purposes.

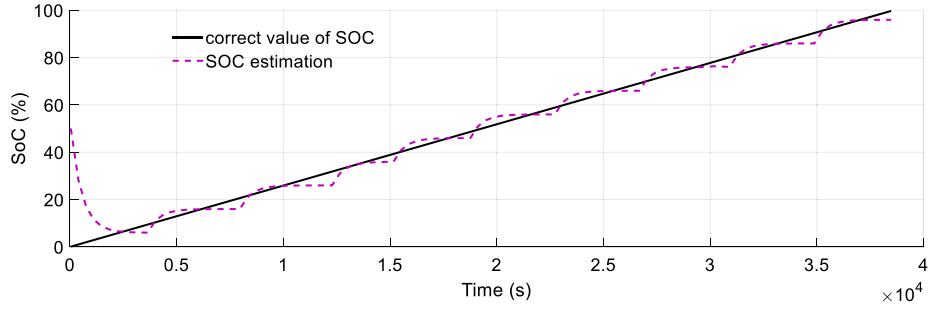

FIGURE 11 Li—S cell SoC estimation using support vector machine (SVM)

The charging features (including both IVFs and TVFs), which were introduced in Section 3, are investigated here for SoH estimation. Since IVFs depend on SoC as well as SoH, they are calculated at a certain SoC level that is assumed to be SoC = 50%. Indeed, the middle charge level is selected because it is the most probable scenario to happen in a real application. According to the results, some features like F1 or F10 have a clear correlation with SoH whereas the others do not show a clear trend. Of course, features with higher correlations (ie, more sensitivity to SoH) are potentially more useful for SoH estimation.

As mentioned earlier, the SVM technique is used for the cell health estimation. To train the SVM model, the collected experimental data is used, and separate sets of data are considered for training and validation. Table 2 presents SoH estimation accuracy using SVM method and different IVF inputs and their combinations. According to the results, individual features F1, F2, F3, and F4 at SoC = 50% are the most promising features. When combining them together, the pairs of (F2, F3) and (F3, F4) give the highest accuracy of 96.4% and 95.8%, respectively. On the other hand, Table 3 shows the SVM results when TVF inputs and their combinations are used. The results demonstrate that F8 and F10 are the best individual features among the TVFs by providing an estimation accuracy of around 95%. When combining them together, the estimation results are clearly improved. Using two features instead of one, the estimation accuracy can potentially increase to more than 96% and this trend continues to more than 97% accuracy when three features are used at the same time. The best result is obtained when all four features are used, which provides an accuracy of 98%.

Figure 12 shows an example result of the cell's health estimation using the SVM and the best input features vs the reference SoH. In that figure, the benchmark is used to evaluate the performance of the proposed SoH estimation technique. Table 3 and Figure 12 show that the SoH estimation technique (ie, feature extraction in combination with SVM) is able to generate reliable outputs, which are comparable with the standard benchmark techniques.

6 | LI—S CELL CAPACITY FADE AND CHARGING EFFICIENCY

The capacity fade of the cell due to cycling is discussed here. Furthermore, the charging efficiency of the cell is calculated. Figure 13 illustrates the capacity fade of the cell due to cycling at 20°C where the cycling test is stopped after 52 cycles because of 20% capacity loss (although more cycling was possible at the cost of more capacity fade). An obvious outcome is that the Li-S battery requires further modifications before commercialization, because of its

TABLE 3 SoH estimation accuracy using SVM method and different TVF inputs and their combinations

Feature	Accuracy (%)	Feature	Accuracy (%)
F_7	91.03	F_9/F_{10}	93.7
F_8	95.36	F_9/F_{12}	92.31
F_9	92.45	F_{10}/F_{12}	93.1
F_{10}	94.8	$F_8/F_9/F_{10}$	96.3
F_{11}	84.33	$F_8/F_{10}/F_{12}$	96.54
F_{12}	92.05	$F_8/F_9/F_{12}$	96.55
F_8/F_9	96.6	$F_9/F_{10}/F_{12}$	97.41
F_8/F_{10}	95.3	$F_8/F_9/F_{10}/F_{12}$	98.06
F_8/F_{12}	96.66		

Abbreviations: SoC, state-of-charge; SoH, state-of-health; SVM, support vector machine; TVF, time-voltage features.

TABLE 2 SoH estimation accuracy using SVM method and different IVF inputs and their combinations

	Input features					
	F_1	F_2	F_3	F_4	F_5	F_6
Accuracy (SoC = 100%)	85.7%	77.6%	92.1%	87.8%	80.6%	74.7%
Accuracy (SoC = 75%)	94.1%	87.8%	91.9%	88.2%	76.5%	81.1%
Accuracy (SoC = 50%)	94.76%	96.1%	95.4%	96.32%	86.02%	82.6%
Accuracy (SoC = 25%)	86.84%	83.75%	94.3%	93.8%	89.1%	85.3%
	F_1/F_2	F_1/F_3	F_1/F_4	F_2/F_3	F_2/F_4	F_3/F_4
Accuracy (SoC = 50%)	93.3%	90.50%	94.2%	96.4%	94.9%	95.8%
	$F_1/F_2/F_3$	$F_1/F_2/F_4$	$F_2/F_3/F_4$	$F_1/F_2/F_3/F_4$		
Accuracy (SoC = 50%)	95.8%	92.8%	92.2%	93.1%		

Abbreviations: IVF, instantaneous voltage features; SoC, state-of-charge; SoH, state-of-health; SVM, support vector machine.

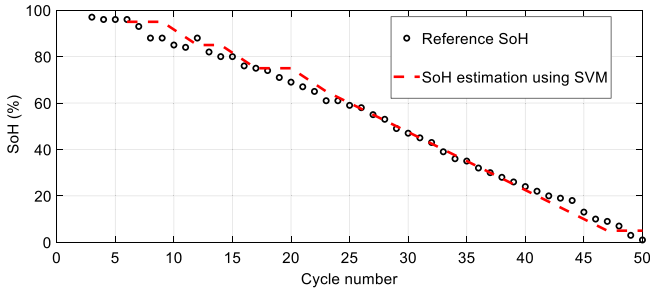

FIGURE 12 Li—S cell SoH estimation using support vector machine (SVM) technique against the reference SoH

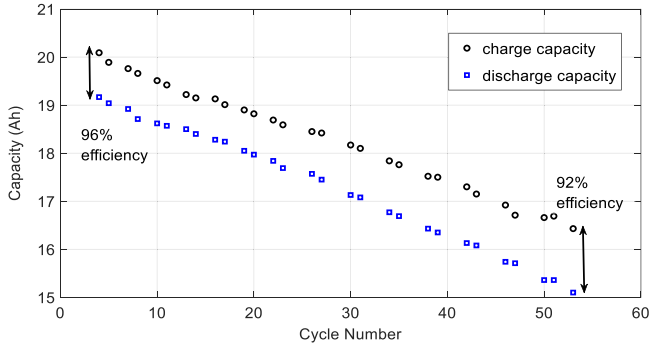

FIGURE 13 Li—S cell charge/discharge capacity during a cycling test

limited cycle life.[4] That is currently restricting its applications in EVs as well as many others.[1,37] In the following, some of the recent publications in that area are reviewed briefly, but before that, an analysis of the cell charging efficiency is presented.

Here, charging efficiency (E_{Ch}) is simply defined by Equation (11) in which Q_{Disch} is the whole discharge capacity, and Q_{Ch} stands for the charging capacity. Both the charge and discharge capacities are calculated at every single cycle of the aging tests. Simply speaking, the charging efficiency is calculated as the ratio of the electricity that we get out of the cell, divided by the electricity that we put into the cell at each cycle.

$$E_{Ch} = \frac{Q_{Disch}}{Q_{Ch}} \tag{11}$$

Figure 13 demonstrates both the charge and discharge capacities during a cycling test at 20°C. As shown in that figure, the charging efficiency is around 96% for a fresh cell whereas that number decreases to 92% after 52 cycles.

As discussed in Reference [38], the key causes of Li—S cell's rapid capacity fade are: (a) low electrical conductivity of sulfur and Li_sS_2/Li_2S, which can lead to a decrease in utilization of active sulfur material and consequently issues in power capability.[39] (b) formation and accumulation of nonconductive films (Li_sS_2/Li_2S) on sulfur cathode, which decreases the electrochemical reaction sites and results in capacity fade.[38] (c) intermediate soluble polysulfide, which can diffuse from cathode to the electrolyte and thus, it reduces the overall quantity of sulfur in the cathode leading to a decrease in battery capacity.[40] In addition, it can diffuse to the Li-anode, reducing to Li_sS_2/Li_2S, and deposit in Li-anode surface.[41] (d) the shuttle effect has been explained in different ways in the literature. According to Reference [42], the consumption of active sulfur materials by the uncontrollable deposition layers causes a higher resistance and rapid capacity fade. Self-discharge happens due to the shuttle effect, which makes the charging time toward infinity and consequently decreasing the efficiency and cycle life of the battery.[42]

Expanding all the above-mentioned research findings here is out of the scope of this study but to summarize them, it should be noted that the literature shows a number of great achievements recently in this field.[1,5] For example in Reference [8], development of a prototype Li—S cell with more than 1000 cycles is mentioned. Although different generations of Li—S prototype cells might be distinct from each other in terms of materials used inside the cell, and their cycle life, we believe that very similar BMS software can be applied to all of them. In fact, their similarities in the shape of voltage curves and state observability, make the present study or other similar studies to be used for future generations of Li-S cells even with much higher cycle life.

7 | CONCLUSIONS

For the first time, charging behavior of a Li—S cell was investigated and characterized for state estimation. Charging features were analyzed at various temperatures and age levels by running a comprehensive set of experiments on a state-of-the-art Li—S cell. Furthermore, a state observability analysis was performed for the Li—S cell to mathematically demonstrate its distinction from the other types of battery. According to the observability calculations, the Li—S cell model is unobservable at various charge levels. That justifies the necessity of developing unique BMS algorithms for this particular type of battery.

In the next step, new state estimators were designed and validated to be used during Li—S cell charging as complementary algorithms in BMS. The SVM and feature extraction techniques were combined to design the Li—S state estimators. The proposed state estimators were then validated against experimental data. According to the

results, the proposed estimators could provide an acceptable level of accuracy during charging with less than 3% error in SoC estimation and less than 2% error in SoH estimation. It is expected that the outcomes of this study will be merged with the existing state estimators, which have been designed to work during cell discharge. Considering the complexities of the Li—S battery state estimation problem in comparison to the Li-ion batteries, having separate state estimators for charge and discharge phases is a wise strategy to reduce the overall errors.

Finally, capacity fade and charging efficiency of the prototype Li—S cells were analyzed based on experimental data. The charging efficiency was obtained around 96% and 92% for a fresh and aged cell, respectively. In addition, the limited cycle life of Li—S cell was discussed based on recent breakthroughs in the literature. Although the next generations of Li—S battery are expected to be different in terms of their lifetime, the outcomes of this study are supposed to remain usable for them as well, because of their similarities in terms of voltage curves and state observability.

ACKNOWLEDGMENTS

The authors thank OXIS Energy for their help and support. This work was funded by the European Commission under grant agreement 814471 and Innovate UK under grant TS/R013780/1.

CONFLICT OF INTEREST

The authors declare no competing interests.

DATA AVAILABILITY STATEMENT

The data that support the findings will be available in Research data for Lithium-Sulfur Cell State of Charge at https://doi.org/10.17862/cranfield.rd.16482957 following an embargo from the date of publication to allow for commercialization of research findings. It is subject to an embargo and will be available from September 1, 2032.

ORCID

Neda Shateri https://orcid.org/0000-0002-5302-3949
Daniel J. Auger https://orcid.org/0000-0002-6199-4251
Abbas Fotouhi https://orcid.org/0000-0002-5402-8629

REFERENCES

1. Dörfler S, Walus S, Locke J, et al. Recent Progress and emerging application areas for lithium–sulfur battery technology. *Energ Technol*. 2021;9(1):2000694.
2. Fotouhi A, Auger DJ, O'Neill L, Cleaver T, Walus S. Lithium-sulfur battery technology readiness and applications—a review. *Energies*. 1937;2017:10.
3. Yuan H, Peng H-J, Huang J-Q, Zhang Q. Sulfur redox reactions at working interfaces in lithium–sulfur batteries: a perspective. *Adv Mater Interfaces*. 2019;6(4):1802046.
4. Hofmann AF, Fronczek DN, Bessler WG. Mechanistic modeling of polysulfide shuttle and capacity loss in lithium-sulfur batteries. *J Power Sources*. 2014;259:300-310.
5. Robinson JB, Xi K, Kumar RV, et al. Roadmap on lithium sulfur batteries. *J Phys Energy*. 2021;3:031501.
6. Takeuchi T, Kojima T, Kageyama H, et al. All-solid-state lithium-sulfur batteries using sulfurized alcohol composite material with improved coulomb efficiency. *Energ Technol*. 2019;7:1900509.
7. Azaceta E, García S, et al. Particle atomic layer deposition as an effective way to enhance Li-S battery energy density. *Energ Technol*. 2020;8:1901432.
8. Huang Y, Shaibani M, Gamot TD, et al. A saccharide-based binder for efficient polysulfide regulations in Li-S batteries. *Nat Commun*. 2021;12:5375.
9. Benveniste G, Rallo H, Canals Casals L, Merino A, Amante B. Comparison of the state of lithium-sulphur and lithium-ion batteries applied to electromobility. *J Environ Manage*. 2018;226:1-12.
10. Fotouhi A, Auger DJ, Propp K, Longo S. Lithium-sulfur battery state-of-charge observability analysis and estimation. *IEEE Trans Power Electron*. 2018;33(7):5847-5859.
11. Fotouhi A, Auger DJ, Propp K, Longo S. Accuracy versus simplicity in online battery model identification. *IEEE Trans Syst Man Cybern Syst*. 2016;48(2):195-206.
12. Fotouhi A, Auger DJ, Propp K, Longo S. Electric vehicle battery parameter identification and SOC observability analysis: NiMH and Li-S case studies. *IEEE Trans Power Electron*. 2017;10(11):1289-1297.
13. Propp K, Auger DJ, Fotouhi A, Longo S, Knap V. Kalman-variant estimators for state of charge in lithium-sulfur batteries. *J Power Sources*. 2017;343:254-267.
14. Propp K, Auger DJ, Fotouhi A, Marinescu M, Knap V, Longo S. Improved state of charge estimation for lithium-sulfur batteries. *J Energy Storage*. 2019;26:100943.
15. Shateri N, Shi Z, Auger DJ, Fotouhi A. Lithium-sulfur cell state of charge estimation using a classification technique. *IEEE Trans Veh Technol*. 2020;70(1):212-224.
16. Xu C, Cleary T, Wang D, Li G, et al. Online state estimation for a physics-based lithium-sulfur battery model. *J. of Power Sources*. 2021;489:229-495.
17. Huang Z, Zhang D, Couto LD, Yang Q-H, Moura SJ. State estimation for a zero-dimensional electrochemical model of lithium-sulfur batteries. *arXiv:2101.10436*. 2021. American Control Conference (ACC). New Orleans, LA, USA: IEEE. https://doi.org/10.23919/ACC50511.2021.9483225
18. Knap V, Stroe D-I, Purkayastha R, et al. Reference performance test methodology for degradation assessment of lithium-sulfur batteries, journal of the electrochemical society. *J Electrochem Soc*. 2018;165(9):1601-1609.
19. Knap V, Stroe D-I, Purkayastha R, Schaltz E. Methodology for assessing the lithium-sulfur battery degradation for practical applications. *ECS Transactions*. 2018;77(11):479-490.
20. Knap V, Auger DJ, Propp K, Fotouhi A, Stroe D-I. Concurrent real-time estimation of state of health and maximum available power in lithium-sulfur batteries, energies. *Energies*. 2018;11(8):2133.
21. Shateri N, Auger DJ, Fotouhi A, Brighton J. An experimental study on prototype lithium-sulfur cells for ageing analysis and state-of-health estimation. *IEEE Trans Transp*. 2021;7(3):1324-1338.

22. Vidal C, Malysz P, Kollmeyer P, Emadi A. Machine learning applied to electrified vehicle battery state of charge and state of health estimation: state-of-the-art. *IEEE Access*. 2021;8:52796-52814.
23. Klass V, Behm M, Lindbergh G. A support vector machine-based state-of-health estimation method for lithium-ion batteries under electric vehicle operation. *J Power Sources*. 2014;270:262-272.
24. Meng J, Cai L, Luo G, Stroe D-I, Teodorescu R. Lithium-ion battery state of health estimation with short-term current pulse test and support vector machine. *Microelectron Reliab*. 2018;88:1216-1220.
25. Deng Y, Ying H, E J, et al. Feature parameter extraction and intelligent estimation of the state-of-health of lithium-ion batteries. *Energy*. 2019;176:91-102.
26. Shu X, Li G, Shen J, Lei Z, Chen Z, Liu Y. A uniform estimation framework for state of health of lithium-ion batteries considering feature extraction and parameters optimization. *Energy*. 2020;204:117957.
27. Guo P, Cheng Z, Yang L. A data-driven remaining capacity estimation approach for lithium-ion batteries based on charging health feature extraction. *J Power Sources*. 2019;412:442-450.
28. Kong J, Yang F, Zhang X, Pan E, Peng Z, Wang D. Voltage-temperature health feature extraction to improve prognostics and health management of lithium-ion batteries. *Energy*. 2021;223:120114.
29. Our cell and battery technology advantages. http://www.oxisenergy.com, accessed on May 29, 2022.
30. Salameh ZM, Casacca MA, Lynch WA. A mathematical model for lead-acid batteries. *IEEE Trans Energy Convers*. 1992;7(1):93-98.
31. Yung WK, Man KF. Optimal selected forgetting factor for RLS estimation. *IFAC Proc*. 1993;26(2):331-334.
32. Ogata K. *Modern Control Engineering*. 5th ed. Englewood Cliffs, NJ: Prentice-Hall; 2010.
33. Ben-Hur A, Horn D, Siegelmann H, Vapnik VN. Support vector clustering. *J Mach Learn Res*. 2001;2:125-137.
34. Steinwart I, Christmann A. *Support Vector Machines*. New York, NY: Springer; 2008.
35. Pattipati B, Sankavaram C, Pattipati K. System identification and estimation framework for pivotal automotive battery management system characteristics. *IEEE Trans. Syst 2011, Man, Cybern, Part C: Appl and Rev*. 200141:869-884.
36. Hu X, Feng F, Liu K, Zhang L, Xie J, Liu B. State estimation for advanced battery management: key challenges and future trends. *Renew Sustain Energy Rev*. 2019;114:109334.
37. Lam L, Bauer P. Practical capacity fading model for Li-ion battery cells in electric vehicles. *IEEE Trans Power Electron*. 2013;28(2):5910-5918.
38. Yan J, Liu X, Li B. Capacity fade analysis of sulfur cathodes in lithium–sulfur batteries. *Adv Sci (Weinh)*. 2016;3(12):1600101.
39. Barchasz C, Molton F, Duboc C, Lepretre J-C, Patoux S, Alloin F. Lithium/sulfur cell discharge mechanism: an original approach for intermediate species identification. *Anal Chem*. 2012;84:3973-3980.
40. Zheng J, Lv D, Gu M, et al. How to obtain reproducible results for lithium sulfur batteries? *J Electrochem Soc*. 2013;160:A2288-A2292.
41. Mikhaylik YV, Akridge JR. Polysulfide shuttle study in the Li/S battery system. *J Electrochem Soc*. 2004;151:A1969.
42. Cañas NA, Wolf S, Wagner N, Friedrich KA. In-situ X-ray diffraction studies of lithium–sulfur batteries. *J Power Sources*. 2013;226:313-319.

How to cite this article: Shateri N, Auger DJ, Fotouhi A, Brighton J. Charging characterization of a high-capacity lithium-sulfur pouch cell for state estimation: An experimental approach. *Energy Storage*. 2022;e412. doi:10.1002/est2.412